INTERFACE

royalsocietypublishing.org/journal/rsif

Research

Cite this article: Bhusari SA, Sharma V, Bose S, Basu B. 2019 HDPE/UHMWPE hybrid nanocomposites with surface functionalized graphene oxide towards improved strength and cytocompatibility. *J. R. Soc. Interface* **16**: 20180273.
http://dx.doi.org/10.1098/rsif.2018.0273

Received: 20 April 2018
Accepted: 20 December 2018

Subject Category:
Life Sciences–Engineering interface

Subject Areas:
biomaterials, bioengineering

Keywords:
cytocompatibility, graphene oxide, high-density polyethylene/UHMWPE blend, mechanical properties, nanocomposites, melt-extrusion

Authors for correspondence:
Suryasarathi Bose
e-mail: sbose@iisc.ac.in
Bikramjit Basu
e-mail: bikram@iisc.ac.in

†These authors contributed equally to the study.

Electronic supplementary material is available online at https://dx.doi.org/10.6084/m9.figshare.c.4380275.

THE ROYAL SOCIETY PUBLISHING

HDPE/UHMWPE hybrid nanocomposites with surface functionalized graphene oxide towards improved strength and cytocompatibility

Shardul Atul Bhusari[1,†], Vidushi Sharma[1,†], Suryasarathi Bose[2] and Bikramjit Basu[1,3]

[1]Laboratory for Biomaterials, Materials Research Centre, [2]Department of Materials Engineering, and [3]Centre for Biosystems Science and Engineering, Indian Institute of Science, Bangalore 560012, India

BB, 0000-0001-7454-368X

High-density polyethylene (HDPE)-based and ultra-high molecular weight polyethylene (UHMWPE)-based composites with carbonaceous reinforcements are being widely investigated for biomedical applications. The enhancement of material properties critically depends on the nature, amount and compatibility of the reinforcement with the polymeric matrix. To this end, this study demonstrates the efficacy of a 'dual' hybrid approach of incorporating modified inorganic nanofiller into an optimized polyethylene blend. In particular, a unique synthesis strategy was adopted to design a covalently bonded maleated polyethylene (mPE) grafted modified graphene oxide (mGO) hybrid nanocomposite. In this scheme, polyethyleneimine (PEI) was initially attached onto GO to synthesize amine functionalized GO (GO–PEI). This is followed by mPE grafting, resulting in mGO. Melt-extrusion together with injection moulding of a polymer mix (60% HDPE–40% UHMWPE) with different proportions (less than or equal to 3 wt%) of surface functionalized GO was conducted to develop nanocomposites of different sizes and shapes. When compared with unreinforced PE blend, the nanocomposites with 1 wt% mGO exhibited an increase in ultimate tensile strength by 120% (up to 65 MPa) and elastic modulus by 40% (up to 908 MPa). The uniform dispersion of modified GO nanofillers, confirmed using X-ray micro-computed tomography and transmission electron microscopy, facilitated effective interfacial adhesion and compatibility with the hybrid polymer matrix. The variation in mechanical properties with GO/mGO addition to PE blend was critically discussed in reference to the structural modification of GO, crystallinity and nature of dispersion of fillers. Importantly, the nanocomposites support the attachment and proliferation of C2C12 murine myoblast cells over 3 days in culture in a statistically insignificant manner with respect to polymer blends without any nanofiller. Taken together, the experimental results suggest that HDPE/UHMWPE/mGO is a promising biomaterial for bone tissue engineering applications.

1. Introduction

The use of orthopaedic implants has increased dramatically during past few decades for fixation of long bones, correction of spinal fractures, replacement of arthritic joints and dental applications [1–4]. The major objectives of the orthopaedic implants are to provide mechanical stability, to facilitate optimal function during physiological loading of bones/joints and to provide desired interactions with the surrounding tissues and musculoskeletal environment [2–5]. The mechanical properties of the implanted materials must be similar to the natural bone to avoid biomechanical mismatch of elastic modulus, causing interfacial instability, especially in the case of hip and knee joints [6,7].

Polymeric materials are widely used in biomedical applications, like artificial joints [8], acetabular cup component [9], tissue scaffolds, etc. [10,11]. In particular, ultra-high molecular weight polyethylene (UHMWPE), owing to its high wear resistance, low coefficient of friction, high impact resistance and toughness, good abrasion resistance and good chemical resistance, has been widely used in many orthopaedic applications, like total hip joint replacement [8,12–15]. Owing to its high molecular weight, UHMWPE has high viscosity, making it difficult to process by conventional screw-extrusion or injection moulding [16]. The poor processability hinders the extensive hybridization of UHMWPE [16]. On the contrary, high-density polyethylene (HDPE) has good processability [16]. Moreover, HDPE is also a biocompatible polymer and is extensively used in biomedical applications [6,16]. It is also reported in the literature that HDPE helps to improve the creep resistance and processability, when blended with UHMWPE [12,15].

Clinically, it has been recognized that wear particle accumulation over time can lead to osteolysis, causing bone loss and implant loosening [5,6,17–20]. This is one of the primary causes of failure of total hip joint replacement surgeries, leading to the requirement of revision operations [17,21]. One of the potential approaches to circumvent this problem and also to further improve the mechanical properties of the polymeric implants is to use inorganic fillers [8,10,22]. For effective reinforcement, factors like uniform distribution of the nanofillers, alignment and efficient stress transfer in the polymer matrix are essential parameters [10,23]. The grafting of polymers onto these reinforcing fillers is an effective method to improve polymer–filler interfacial adhesion and in turn, the mechanical and cytocompatibility properties of the composite [6,11,23,24]. In a limited number of studies, the researchers investigated the role of MWCNT or carbon nanofibres or hydroxyapatite (HA) on the processing, mechanical and tribological properties of UHMWPE or HDPE/UHMWPE hybrid composites [12,15,16,25]. However, the role of GO or chemically modified GO on mechanical and cytocompatibility property of UHMWPE/HDPE hybrids are not yet reported.

Graphene, a new class of two-dimensional carbon nanostructure, has garnered significant interest due to its excellent electronic, mechanical and thermal properties [11,26,27]. Many applications of graphene and its derivatives have been explored in the field of targeted drug delivery [28], bioimaging [29], antibacterial treatments [30], orthopaedic applications [6], cancer therapy [29,31], etc. Also, graphene oxide (GO), due to the presence of functional groups, is compatible with polymers [11]. Recently, incorporation of GO nanofillers into different biopolymers has given rise to exceptional mechanical properties and biocompatibility [8,32]. The hydrophobic π domains in the core region and ionized groups, like carboxylic acid, hydroxyl and epoxide groups around the edges of GO, enhances its interactions with proteins through hydrophobic and electrostatic interactions [6,8,26,27,33]. However, as-synthesized GO tends to form many aggregations due to the strong van der Waals forces and, in turn, limit the load transfer from the polymer matrix to the nanofillers [34]. Many surface functionalization techniques are effective in overcoming this hurdle, but the complicated synthesis and chemical treatments involved may hamper the cost-effectiveness and process scalability [34]. On the other hand, the covalently grafted polymer chains onto the nanofillers will lead to easy mixing into the polymer matrix and improved interface, thus providing a convenient way to achieve the reinforcement and better mechanical properties [6,34–36].

In the present study, we have developed a new strategy to graft polyethylene chains onto the surface of GO to improve the structural properties and investigate its cytocompatibility. The base polymer matrix is an optimized blend of 60% HDPE and 40% UHMWPE (HU) to achieve good processability. Instead of alternative techniques for polymer processing like solvent casting and pressurized gyration [37], melt-extrusion, a solvent-free [38,39] technique, was used to blend the composites in the present work [40,41]. In this scalable processing approach, the nanocomposite was thermoplastically extruded at elevated temperatures and injection moulded in the desired shape. The modified GO (mGO), prepared by the aforementioned process, is expected to achieve homogeneous dispersion, to cause stronger interactions and to enhance the load transfer from the polymeric matrix to graphene. Therefore, efforts were made to enhance the mechanical properties of HDPE-based and UHMWPE-based composites, wherein surface-modified GO were melt-mixed. Further, structural and mechanical properties of the nanocomposites were investigated along with evaluation of viability, proliferation and attachment of C2C12 mouse myoblast cells to assess the applicability of these materials in biomedical.

2. Material and methods

GO nano-powder was obtained from Bottom Up Technologies Corporation (India). UHMWPE (average molecular weight: 3×10^6 to 6×10^6 g mol^{-1}), HDPE (melt index: 2.2 g 10 min^{-1}), maleated polyethylene (mPE), branched polyethyleneimine (PEI, molecular mass 25 kDa), 1-ethyl-3-[3-(dimethylamine)propyl]-carbodiimide hydrochloride (EDC), *N*-hydroxysuccinimide (NHS) and WST-1 assay were obtained from Sigma-Aldrich (USA). Triethylamine (TEA), xylene and ethanol were obtained from Merck (India).

2.1. Synthesis of amine functionalized graphene oxide

Amine functionalized GO was synthesized by conjugating PEI to the carboxyl groups of GO by EDC/NHS coupling [27]. Dried GO was dispersed in deionized water by sonication for 45 min. EDC (54.3 mg, 0.4 mmol) and NHS (50.6 mg, 0.4 mmol) were added to the GO solution (0.5 g ml^{-1}, 0.5 g). TEA (100 µl) was added to the PEI solution (0.396 g) in deionized water. Further, the PEI solution was added to the GO solution and stirred for 1 day at room temperature. The resulting GO–PEI solution was centrifuged and washed in TEA to remove unreacted PEI and prevent its release during the cell culture studies and thus prevent toxicity.

2.2. Synthesis of modified graphene oxide

GO–PEI and mPE were dispersed in xylene and refluxed for 1 h at 100°C. The weight ratio of GO–PEI and mPE was 1 : 3 to ensure complete conversion of amine groups of GO–PEI to imide groups [4]. The solution was then centrifuged and washed in xylene to remove unreacted mPE and get mGO. Scheme 1 shows the different steps involved in the mGO synthesis.

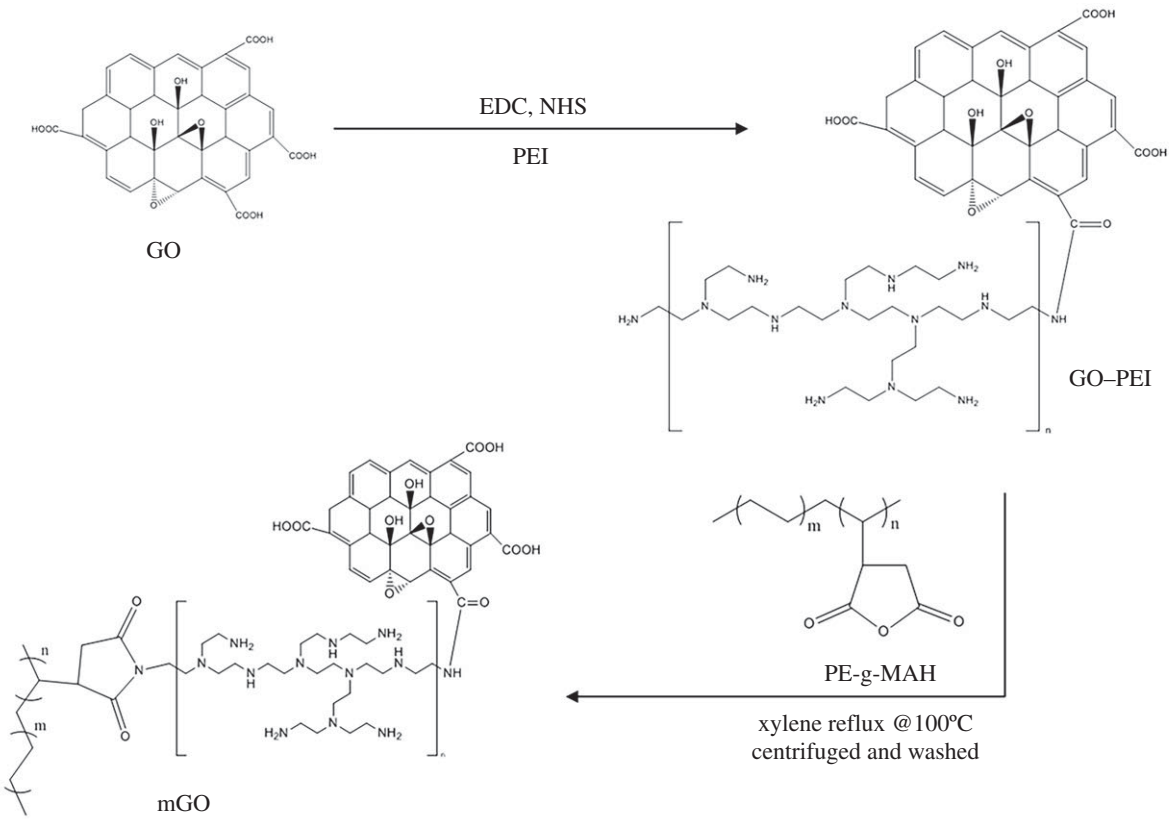

Scheme 1. Surface modification of GO enhances its compatibility with the polymer blend. Synthetic approach followed by grafting of polyethylene on GO. PEI, polyethyleneimine; EDC, 1-ethyl-3-[3-(dimethylamine)propyl]carbodiimide hydrochloride; NHS, *N*-hydroxysuccinimide; PE-g-MAH, polyethylene-grafted maleic anhydride; mGO, modified GO.

2.3. Melt-extrusion of modified graphene oxide-reinforced high-density polyethylene/ultra-high molecular weight polyethylene nanocomposites

The nanocomposites consisted of 60% HDPE and 40% UHMWPE (HU) reinforced with 0.5, 1 and 3 neat GO and 0.5, 1 and 3% modified GO (table 1). The nanocomposites were melt-mixed in DSM Xplore MC 15 melt extruder at a temperature of 220°C and screw speed of 60 rpm for a duration of 10 min. The blend was mixed for 10 min as a stable force of *ca* 6 kN was reached with time (electronic supplementary material, figure S1).

The extruded nanocomposites were subsequently injection moulded in Xplore Microinjection Moulding Machine at an injection pressure of 12 bar with melt temperature at 220°C and mould temperature at 100°C to get dumbbell-shaped specimens using the ASTM D638-03 Type 5 standard.

Table 1. Composition of graphene-reinforced HDPE/UHMWPE nanocomposites.

hybrid composite grade	HDPE (wt%)	UHMWPE (wt%)	GO (wt%)	mGO (wt%)
HU	60	40	—	—
0.5 GO	60	40	0.5	—
0.5 mGO	60	40	—	0.5
1 GO	60	40	1	—
1 mGO	60	40	—	1
3 GO	60	40	3	—
3 mGO	60	40	—	3

2.4. Structural analysis of graphene oxide, graphene oxide–polyethyleneimine and modified graphene oxide

Dispersed GO nanoparticles were drop casted on a silicon wafer and dried in vacuum to perform atomic force microscopy analysis (AFM, A100, A.P.E.Research) in non-contact mode. XRD patterns of GO, GO–PEI and mGO were recorded by PANalytical (The Netherlands) X-ray diffractometer with Cu Kα radiation ($\lambda = 0.154$ nm) and Ni filter with a step size of 0.02° and a low scan rate of 0.25° min^{-1}. The attenuated total internal reflection Fourier transform infrared spectra (ATR-FTIR, Bruker) of GO, GO–PEI and mGO were recorded from 4500 to 800 cm^{-1}. More complimentary structural characteristics of GO, GO–PEI and mGO were carried out using Horiba LabRAM HR Raman Spectrometer with a 532 nm monochromatic laser.

2.5. Thermal characterization of modified graphene oxide and determination of crystallinity

The percentage grafting of polyethylene was calculated using a thermogravimetry analyser (TGA, TA Instruments). Samples were heated from room temperature to 700°C at a heating rate of 10°C min^{-1} in nitrogen atmosphere. Differential scanning calorimeter (DSC) experiments were carried out using DSC (TA Instruments, Q2000), under inert atmosphere. Melting temperature (T_m), crystallization temperature (T_c), specific heat of fusion (Δh_f) and degree of crystallinity (χ_c) were measured. The samples, weighing between 4 and 7 mg, were subjected to a

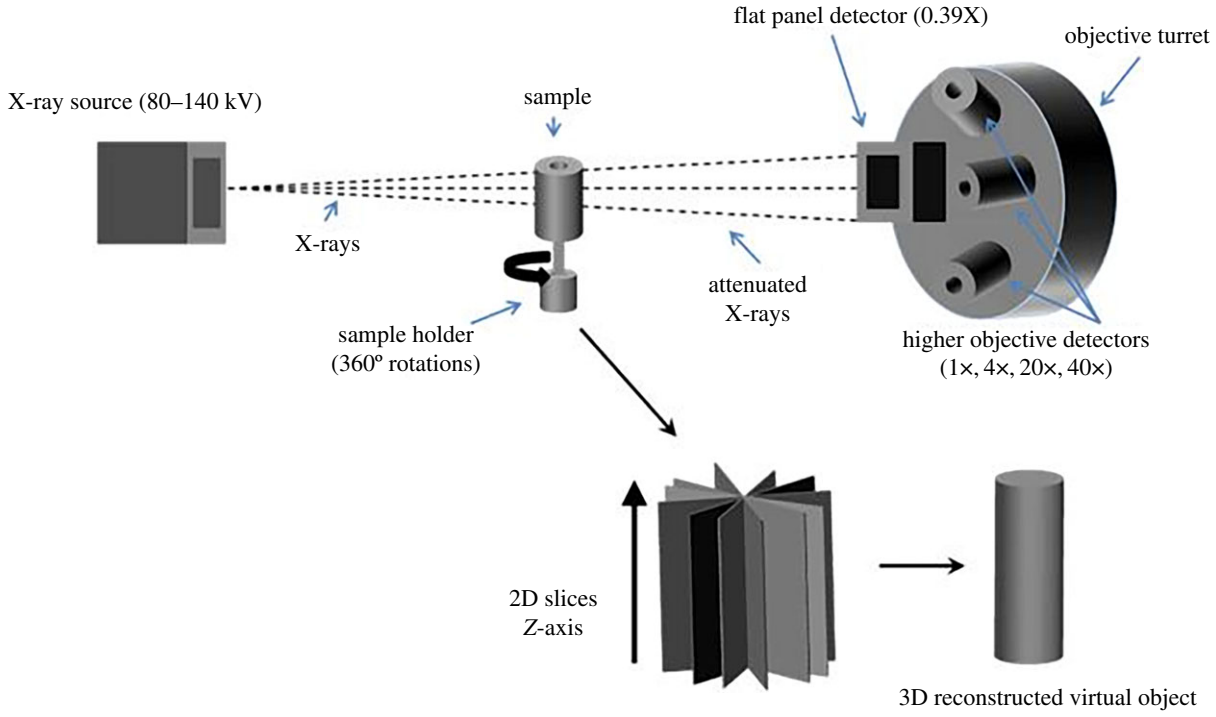

Scheme 2. Schematic diagram showing the principle of virtual volume rendering of X-ray μ-CT. (Online version in colour.)

heating–cooling–heating scan in order to eliminate the thermal histories. The scans were obtained by heating the samples to 200°C, cooling them to −30°C and again heating them to 200°C using heating and cooling rates of 10°C min^{-1}. The DSC endotherms were taken from the second heating cycle. The degree of crystallinity of the samples was calculated according to the following equation:

$$\chi_c\ (\%) = \frac{\Delta h_f}{\Delta h_f^0} \times 100,$$

where Δh_f^0 is the heat of fusion corresponding to 100% crystalline polyethylene, taken as 290 J g^{-1} [42–44].

2.6. Rheological properties of the nanocomposites

Viscoelastic properties of neat blend HU and GO/mGO-reinforced nanocomposites were tested out using a stress-controlled discovery hybrid rheometer (DHR-3, TA Instruments) with parallel plate geometry (25 mm diameter and 1 mm gap distance). For rheological measurements, the samples were prepared by hot pressing at 220°C. Frequency sweep analysis was performed in a frequency range of 100–0.1 rad s^{-1} at 240°C and a fixed strain of 1% which is in the linear viscoelastic region.

2.7. Nanoparticle dispersion in 60% high-density polyethylene and 40% ultra-high molecular weight polyethylene blend

The dispersion of both 1 GO and 1 mGO in the HU blend was analysed with the help of transmission electron microscopy (FEI TECNAI BIO TWIN 12, TEM) at 120 kV. The thin sections (approx. 70 nm) were carefully cut using a cryo-ultramicrotome (RMC Boeckeler, USA) from the extruded strands using a diamond knife and an antistatic holder. During sectioning, the samples and the blade were maintained at an optimized temperature of −120°C and −80°C, respectively.

Three-dimensional structural analysis of selected samples was observed with X-ray micro-computed tomography (μ-CT, VersaXRM-500, Xradia, Zeiss, Germany). The μ-CT is usually carried out by passing X-rays from a source through the sample mounted on the holder. The attenuated X-rays, after being absorbed by the sample, are detected through the different types of detectors (0.39×, 1×, 4×, 20× and 40×). The virtual three-dimensional volume rendering takes place when the sample rotates 360° with respect to the number of projections (scheme 2). In this case, image acquisition was carried out for about 4 h 45 min with 3201 projections at a step size 0.11°. The voltage of the X-ray source was fixed at 70 kV and the corresponding power was 6 W with an exposure time of 3 s. A low energy (LE 1) filter was used in the case of 1 GO while no filter was required for 1 mGO. A combination of 4× objective and a voxel size of approximately 2 μm was used.

2.8. Mechanical characterization

Uniaxial tensile testing was carried out using INSTRON 5967 to measure the engineering stress–strain response and, in particular to assess ultimate tensile strength and elastic modulus. The dumb-bell-shaped specimens, obtained by injection moulding, were tested under a crosshead speed of 5 mm min^{-1} (strain rate = 25 s^{-1}) and loading continued until the specimens fractured. The Halpin–Tsai model was used for the micro-mechanical theoretical prediction of the modulus of the nanocomposites.

Owing to the unavailability of a suitable extensometer, which can be attached to soft materials, like polymers without deforming them at the attachment area, we could not measure the true stress–strain response. Nevertheless, the fracture surface of the nanocomposite samples was analysed using field emission scanning electron microscope (FEI, USA), operated at 5 kV accelerating voltage. Prior to scanning, the samples were coated with a thin layer of gold to minimize the charging effect.

2.9. Cell culture

The samples were sterilized by soaking them in 70% ethanol for 2 h, exposed to UV light for 30 min and then washed with phosphate-buffered saline (1× PBS; pH 7.4) before cell seeding. Sterilized disc shaped HU, 1 GO and 1 mGO samples, prepared using compression moulding with a diameter of *ca* 10 mm

and thickness of 1 mm, were used for the experiment. The mouse myoblast C2C12 cell line was used for all the *in vitro* cytocompatibility experiments.

The cells were revived from cryo-preserved stock prior to seeding and expanded in tissue culture graded T25 flask (Eppendorf, Germany) containing culture media consisting of Dulbecco's modified Eagle's medium (Invitrogen), 15% (v/v) fetal bovine serum (Invitrogen) and 2 mM L-glutamine (Invitrogen), 1% (v/v) antibiotic antimycotic solution (10 U ml^{-1} penicillin and 0.1 mg ml^{-1} streptomycin, Sigma-Aldrich). Cells were maintained in a 5% CO_2 incubator (Sanyo, MCO-18AC, USA) operated at 37°C temperature and 95% humidified atmosphere. The culture media were changed after 2 days. Once the cells reached 70–80% confluency, they were detached from the culture flask using 0.05% trypsin–EDTA (Invitrogen) and subcultured for further use. All the experiments were conducted with cells at passage of 2–7. Gelatin (0.2%)-coated glass coverslips were used as a control sample.

2.9.1. Cell viability using WST-1 assay

Generally, cell viability is quantified using MTT (3(4, 5-dimethylthiazol-2-yl)-2, 5-diphenyltetrazolium bromide) assay. However, the WST-1 (4-[3-(4-iodophenyl)-2-(4-nitrophenyl)-2H-5-tetrazolio]-1, 3-benzene-disulfonate) assay has been reported to have no interaction with GO and also the cleaved tetrazolium product is water-soluble which eliminates the need for the solubilization step followed in MTT assay [4,43]. Thus, WST-1 was preferred over the MTT assay to reliably assess the viability of the myoblasts cells on the nanocomposites.

Approximately, 4×10^3 cells per well of C2C12 myoblast cells were seeded on the sterilized samples placed in 24-well plates and incubated in 5% CO_2 incubator for 1 and 3 days at 37°C and 95% humidified atmosphere. A 400 µl of 10% v/v solution of WST-1 (Roche) assay and complete culture medium was prepared to add to each of the wells. After incubation for 3 h at 37°C in 5% of CO_2 atmosphere along with saturated humidity, the optical density (OD) of the developed colour was measured by a microplate reader (iMark, Biorad Laboratories, India) at a wavelength of 450 nm. The absorbance value provides a direct correlation with the number of viable cells in each well. The measurements were obtained as an average of three wells repeated thrice. Cell viability (%) was calculated using the following formula:

$$\%\ \text{cell viability} = \frac{\text{mean absorbance of the sample}}{\text{mean absorbance of the control}} \times 100.$$

2.9.2. Fluorescence imaging and scanning electron microscopy analysis

In order to analyse and quantify the nuclei of the proliferated active cells, the sterilized samples were placed in a 24-well plate. A total of 4×10^3 cells per well of C2C12 mouse myoblast cells were seeded on the samples. The cells were cultured for 3 days and the samples were then washed thrice with 1× PBS followed by fixation of samples in 3% paraformaldehyde (PFA; SD Fine-Chem Lit) for 30 min. After washing three times with 1× PBS, 0.1% Triton X solution was added and kept for 10 min for permeabilization. The cells were then washed thrice with 1× PBS and blocked with 1% bovine serum albumin (BSA) for 30 min to prevent non-specific binding of dye. Hoechst stain 33342 (Invitrogen) was then added and kept for 20 min to visualize the active nuclei. The samples were then washed with 1× PBS to remove the excess stain and observed under fluorescence microscope (Nikon LV 100D, Japan). The cell count was calculated by capturing images of Hoechst-stained nuclei at 20 different locations of each sample and averaged over the entire substrate area.

For the cell adhesion test, about 4×10^3 cells per well were seeded on the surface of each sterilized sample placed in 24-well plates. After 3 days in culture, the samples were washed with 1× PBS and fixed with 3% glutaraldehyde (LobaChemie, India) in PBS for 30 min at room temperature. A series of ethanol washes (30, 40, 50, 60, 70, 80, 90 and 100% v/v in DI) was done subsequently for 10 min each to dehydrate the samples completely. The samples, dried overnight, were coated with gold via sputtering and observed under field emission scanning electron microscope.

2.10. Statistical analysis

All the *in vitro* experiments were performed in triplicate and replicated thrice. The analysed data were plotted as mean ± standard deviation. Statistical analysis was performed by using SPSS-16.0 (IBM, USA) software. Analysis of variance (ANOVA) test was performed for comparing significant differences in the obtained results. The *p*-value at 0.05 was considered as statistically significant.

3. Results

The methodology involved in surface modification of GO nanosheets and polymer nanocomposite fabrication is mentioned with specific details in the previous section. A novel approach was used to surface functionalize the GO nanosheets with PEI and mPE for better compatibility within the polymer blend. Another challenging task was to process the HDPE/UHMWPE blend in the melt extruder. The 60% HDPE/40% UHMWPE (HU) blend was found to be optimum and the force generated inside the twin-screw extruder, reached stable values, suggesting proper mixing of the blend when compared with other compositions like 50%HDPE/50%UHMWPE blend (discussed in the electronic supplementary material).

3.1. Surface modification of graphene oxide to form modified graphene oxide

Figure 1*a–c* shows the AFM image of GO flakes in non-contact mode. The topography image of GO revealed that the height of GO is *ca* 2 nm [33]. The successful conjugation of PEI and mPE on the GO nanosheets was analysed using XRD and FTIR studies. The characteristic XRD peak (figure 1*d*) of GO was exhibited at $2\theta = 10.8°$ [45,46]. The characteristic X-ray peak for the amine functionalized GO–PEI and mPE functionalized GO is shifted to the left at $2\theta = 10.1°$ and $2\theta = 9.94°$, respectively. This shift can be attributed to the increased interlayer spacing between the GO nanosheets upon incorporation of amine groups and mPE chains [47]. In figure 1*e*, the absorption bands of GO at 1717, 1584, 1165 and 3337 cm^{-1} are attributed to the stretching bonds of C=O (carboxylic groups), –C=C–, the epoxy ring and the hydroxyl group, respectively [6]. The successful conjugation of the carboxyl group of GO and amino group of PEI was confirmed by the diminishing of the peak corresponding to the COOH group and the appearance of the characteristic IR bands of the amide bond at 1622 cm^{-1} (C=O) and 1567 cm^{-1} (N–H) [48]. The absence of the IR band at 1165 cm^{-1} corresponding to the epoxy ring was observed in GO [29]. Also, those present at 2921 and 2852 cm^{-1}, corresponding to alkane $-CH_2$ [22] in GO–PEI, clearly establish successful amine functionalization. The IR bands at 2914 and 2847 cm^{-1} in mGO correspond to the alkane $-CH_2$ bond [22]. In addition, IR bands at 1373 and 1711 cm^{-1} can be attributed to the stretching frequency of imide C–N and imide C=O bonds, respectively. Taken together, the FTIR results establish that polyethylene was successfully grafted on the amine functionalized GO [6,49,50].

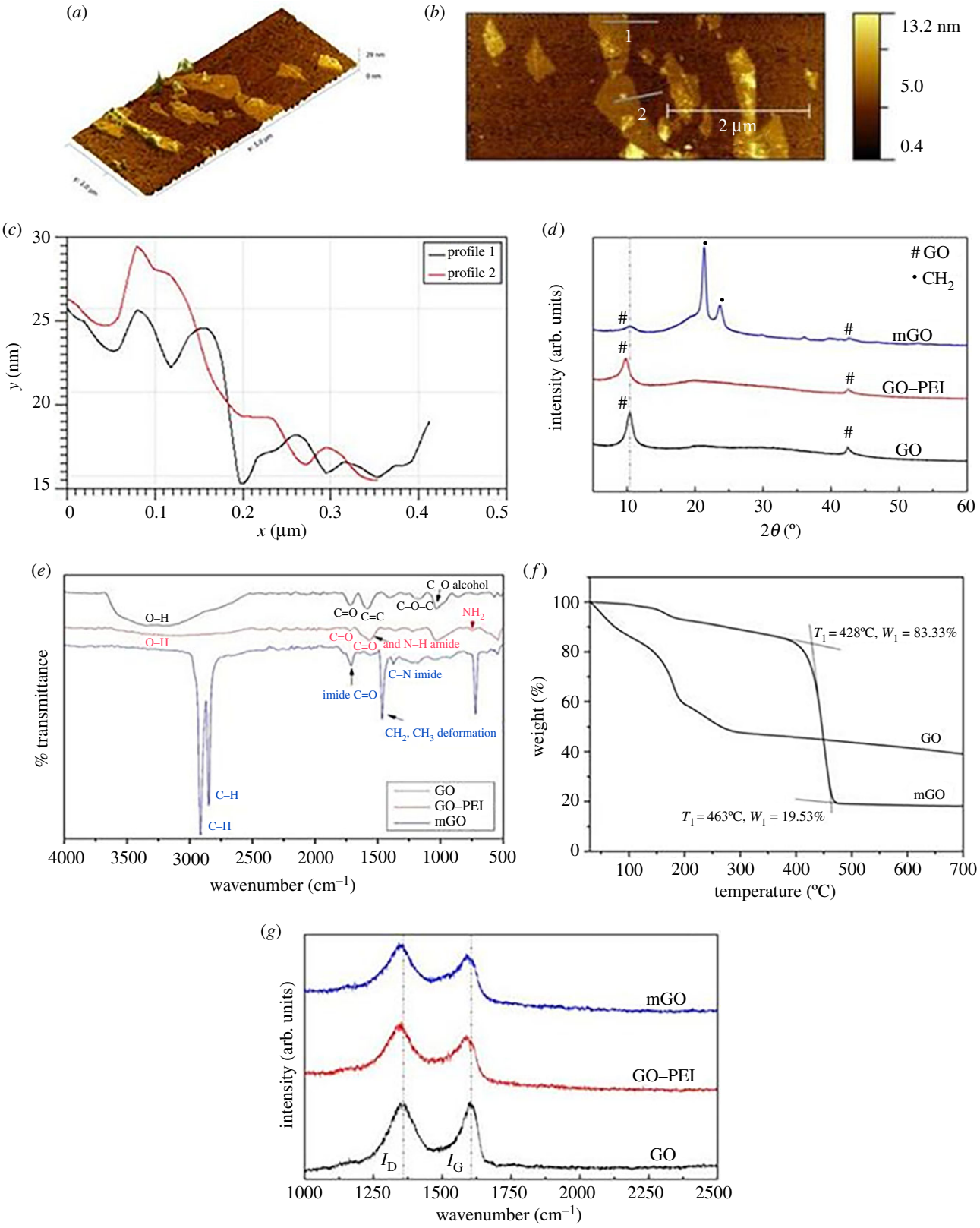

Figure 1. Surface modification of GO and consequent changes in the physico-chemical properties have an effect on the mechanical properties of the hybrid polymeric composites. (*a*) Three-dimensional topography image; (*b*) two-dimensional topography image; (*c*) height profile from AFM; (*d*) XRD pattern of GO, GO–PEI and mGO; (*e*) FTIR spectra for as-synthesized GO, GO–PEI and mGO; (*f*) TGA profile for mGO; (*g*) Raman spectra for as-synthesized GO, GO–PEI and mGO. (Online version in colour.)

In figure 1*g*, the structural changes in GO can be quantified with the help of Raman spectroscopy. A shift in wavenumber (towards the left) as well as peak intensity, especially in the case of the G-band can be observed. The I_D/I_G ratio is 0.96, 1.21 and 1.19 for GO, GO–PEI and mGO, respectively.

3.2. Grafting efficiency of mPE on graphene oxide and crystallinity measurement

The adopted synthesis approach can be effectively used to graft polyethylene onto the GO nanosheets. The grafting efficiency was quantified using thermogravimetric analysis profile for

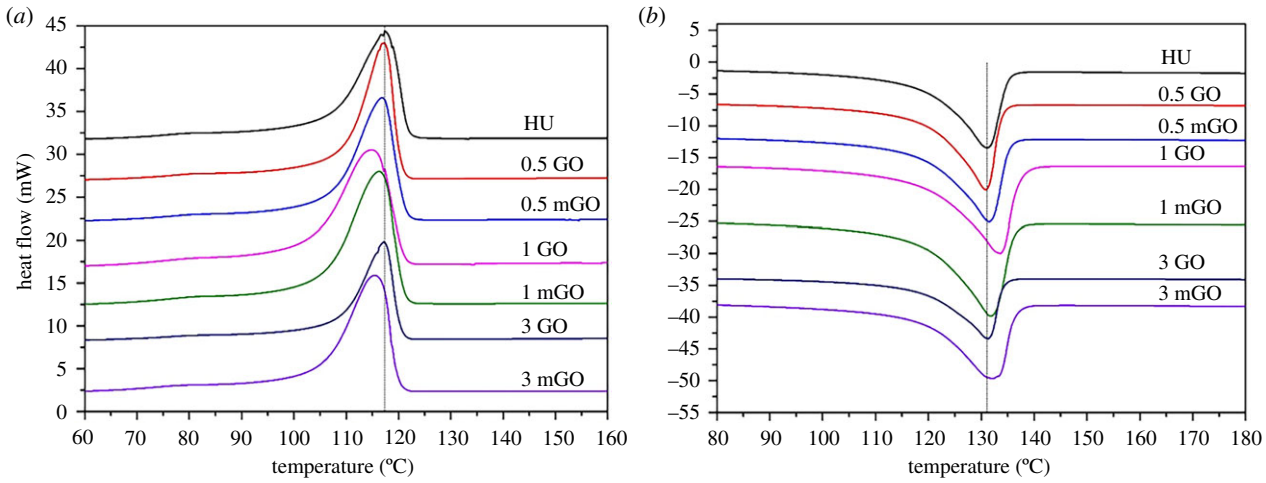

Figure 2. Crystallinity of the HU blend influences the mechanical properties. DSC melting (*a*) endotherms and (*b*) exotherms of HU, GO–HU and mGO–HU nanocomposites. For the material grade compositions mentioned in the figure, refer to table 1. (Online version in colour.)

mGO (figure 1*f*). GO shows a weight loss of approximately 14% at 100°C and approximately 27% at 200°C. This weight loss at 100°C and 200°C is due to evaporation of trapped water molecules and pyrolysis of the oxygen containing functional groups, respectively [36,51,52]. However, mGO did not show significant degradation at 100°C, suggesting increased hydrophobicity due to the presence of polyethylene chains [51]. At 200°C, a weight loss of only approximately 7% was observed due to pyrolysis of the oxygen containing functional groups as opposed to approximately 27% for the same in the case of GO. This proves that the polyethylene chains occupy the oxygen containing functional groups and a sharp weight loss further observed at approximately 400°C was due to the decomposition of the covalently bonded mPE on the amine functionalized GO [51,52]. From the TGA profile, the percentage of grafted polyethylene in mGO was approximately 63.8%, which is independent of GO content. Ideally, the grafting ratio (GR) is defined as the ratio of the weight of the grafted polymer (maleated PE, in this study) to GO, mentioned by Lou *et al.* [53]. In order to calculate the GR of maleated PE on the surface of GO, TGA is found to be the only viable approach to quantify in this case. The major challenge is that the molecular weight for maleated PE is neither reported in the literature nor in the material data sheet. For this grade of maleated PE, a saponification value of 32–36 mg KOH/g is reported generally.

The crystallization parameters of the nanocomposites are summarized in table 2. The melting and crystallization curves of the nanocomposites are depicted in figure 2. The crystallization temperature (T_c) and melting temperature (T_m) of the HU blend did not show much variation with the addition of GO or mGO nanofillers. However, the 1 mGO sample showed a sharp increase in the specific heat of fusion (Δh_f), resulting in the higher degree of crystallinity of *ca* 59%.

3.3. Rheological properties

Melt rheological studies for the HU blends were carried out to observe their flow behaviour and viscoelastic properties. The measurements of rheological properties were carried out at 240°C, which is closer to the processing temperature (220°C) of the blend. Therefore, the recorded data can be used to interpret the influence of nanofiller on the processibility of the polymer blend. The rheological property was analysed with variation in complex viscosity (η^*) as a function of angular frequency (figure 3). It is observed that complex viscosity decreases with increasing angular frequency, a typical characteristic of shear thinning fluids [54]. As seen in figure 3, the variation in viscosity values is within the range of 10^4–10^5 Pa s. HU blend reinforced with 1 wt% of unmodified GO (1 GO) shows the highest viscosity, followed by 0.5 GO. By contrast, HU blend reinforced with mGO shows a decrement in viscosity, leading to enhancement in its processibility. Also, 1 mGO has a cross-over point with HU neat blend at a lower frequency region, as a change in the value of axial force is observed. A similar trend was observed in the case of 3 GO and 3 mGO but with less prominence when compared with 0.5 and 1 wt% loadings.

Table 2. Crystallization parameters of the HU, GO–HU and mGO–HU nanocomposites.

hybrid composite grade	T_c (°C)	T_m (°C)	Δh_f (J g^{-1})	χ_c (%)
HU	117.4	131.0	129.9	44.8
0.5 GO	117.2	130.8	134.7	46.4
0.5 mGO	116.9	131.5	127.9	44.1
1 GO	114.9	133.5	120.4	41.5
1 mGO	116.3	131.9	172.4	59.4
3 GO	117.2	131.2	117.7	40.6
3 mGO	115.5	132.2	115.2	39.8

3.4. Graphene oxide/modified graphene oxide nanofiller dispersion

The uniform dispersion of nanofiller in the matrix is an important aspect to effectively tune the property of the matrix. TEM was carried out to evaluate the dispersion of GO and modified GO in HU blends at the nano-scale. Figure 4 shows representative bright field TEM images for 70 nm electron thin sections of both 1 GO and 1 mGO samples. The black hairy structures

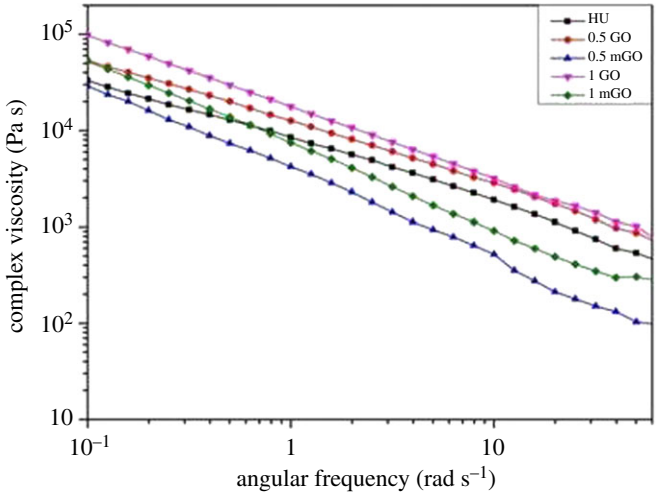

Figure 3. Viscoelastic response affects the dispersion of nanoparticles in the polymeric blend. Variation of complex viscosity as a function of angular frequency for reinforced blends. For the material grade compositions mentioned in the figure, refer to table 1. (Online version in colour.)

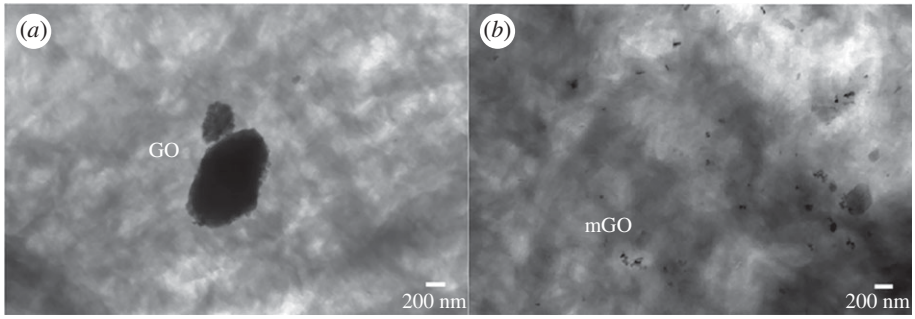

Figure 4. Dispersion of filler in composite effectively enhances the property of the matrix. Representative bright field transmission electron micrographs showing carbonaceous filler distribution in 1 GO (*a*) and 1 mGO (*b*).

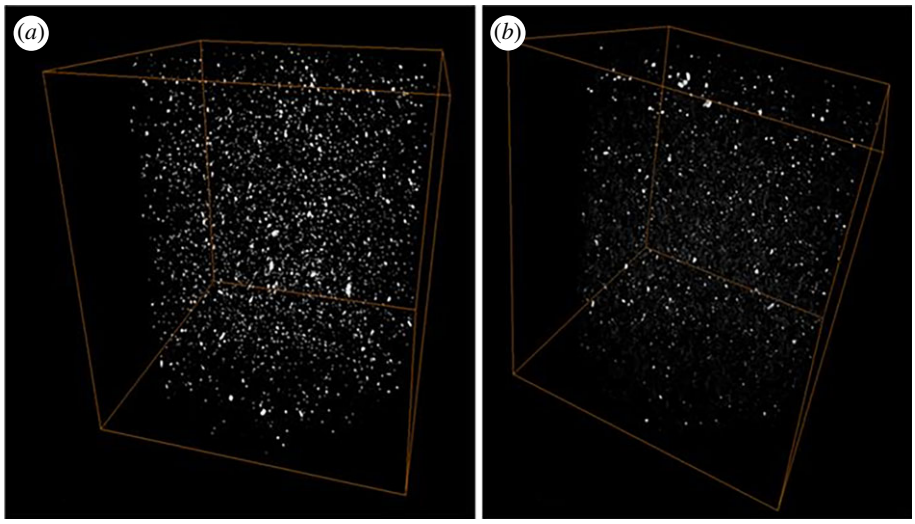

Figure 5. Dispersion of GO/mGO nanofillers within a polymer blend determines its mechanical and surface properties. Microstructural analysis in three-dimensional reconstructed volumes of (*a*) 1 GO and (*b*) 1 mGO. The area of the cubic ROI is 2026.2 × 2026.2 × 2026.2 μm^3.

encompassing the entire image indicate the lamellae of polyethylene, whereas the black particles show the dispersion of modified and unmodified GO, respectively, in figure 4*a*,*b*. The unmodified GO agglomerated with typical agglomerate sizes of 2 μm and dispersed poorly in the HU matrix (figure 4*a*). This is a signature of the poor interaction of polar GO with the non-polar HU matrix. By contrast, the grafting of maleated PE onto GO, modified with PEI, facilitates a better dispersion in the HU matrix (figure 4*b*). A careful look reveals the dispersion of nanometric mGO (50–100 nm) particles within the polymer matrix. With further pre-extrusion modifications on the nanocomposites and fine tuning the extrusion parameters, the dispersion characteristics of mGO can be further improved.

Figure 5 shows three-dimensional volume rendered μ-CT images for both 1 GO and 1 mGO. The area of the cubic region of interest (ROI) is 2026.2 × 2026.2 × 2026.2 μm^3. The images were reconstructed with the help of 'XMReconstructor'

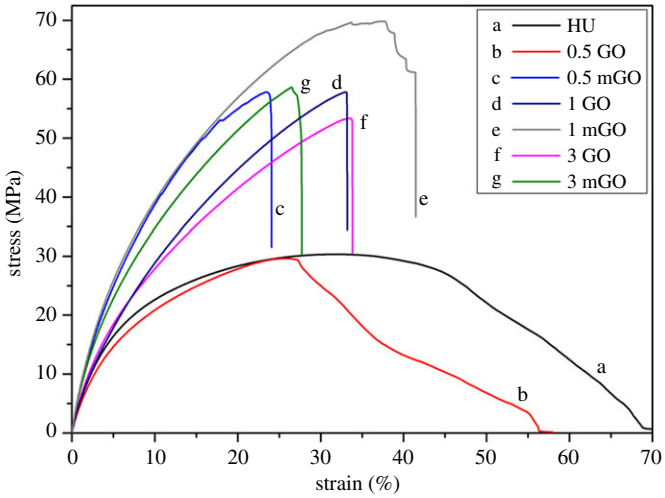

Figure 6. Reinforcement of GO/mGO nanofillers alters the mechanical properties of the polymer blend. Engineering stress–strain plot for HU, GO–HU and mGO–HU nanocomposites. For the material grade compositions mentioned in the figure, refer to table 1. (Online version in colour.)

Table 3. Summary of tensile properties obtained for the HU matrix and its nanocomposites.

hybrid composite grade	ultimate tensile strength (MPa)	elastic modulus (MPa)
HU	29.5 ± 0.6	645.7 ± 41.6
0.5 GO	29.1 ± 2.5	620.0 ± 27.5
0.5 mGO	56.7 ± 0.7	961.3 ± 44.7
1 GO	56.1 ± 3.7	787.7 ± 53.6
1 mGO	65.1 ± 3.4	908.0 ± 58.1
3 GO	55.2 ± 5.3	805.3 ± 70.3
3 mGO	56.3 ± 1.8	835.0 ± 104.7

(Xradia, Zeiss, Germany). The bright particles, which are observed in the rendered volume, are the GO nanoparticles. It is observed that the mGO has been better dispersed in the polymer matrix when compared with the unmodified GO. The formation of agglomerates, seen as a bright phase, is greater in the case of 1 GO (figure 5*a*). For visual clarity of the dispersion of GO nanofillers, the HU blend matrix was masked in the three-dimensional images.

3.5. Ultimate tensile strength and elastic modulus

The uniaxial tensile properties of all the nanocomposites were evaluated using ASTM standards. The representative engineering stress–strain curves for the GO–HU nanocomposites at a crosshead speed of 5 mm min^{-1} are shown in figure 6. The ultimate tensile strength and the elastic modulus of HU were found to be *ca* 29 MPa and 645 MPa, respectively. The addition of 0.5, 1 and 3 wt% of unmodified GO and mGO to the HU blend resulted in significant differences in the mechanical properties, as tabulated in table 3. In the 0.5 GO sample, no significant improvement in the mechanical properties was recorded when compared with the HU blend. However, in the case of 0.5 mGO reinforcement, the ultimate tensile strength reached *ca* 56.7 ± 0.7 MPa and an elastic modulus of *ca* 961 ± 45 MPa, showing significant enhancement of the mechanical properties. The 1 mGO sample showed a sharp increase of 120% (*ca* 65.1 ± 3.3 MPa) in the ultimate tensile strength and 40% (*ca* 908 ± 58 MPa) in the elastic modulus, when compared with that of the HU sample. Although the 1 GO sample showed comparable ultimate tensile strength to that of 0.5 mGO, the elastic modulus of the latter was better. A further increase in the GO and mGO nanofiller loading to 3%, however, reduced the ultimate tensile strength and elastic modulus both, compared to 1% loading. This indicates that dispersion at higher loading of fillers can potentially lower the mechanical properties.

Scanning electron microscopy (SEM) analysis was used to investigate the fracture surface morphology in the presence and absence of GO in the HU blend. From figure 7*a*, it can be seen that the HU sample exhibited a fibrous fracture morphology. Also, the 0.5 GO nanocomposite, which was found to have similar mechanical properties to that of HU, showed a fibrous morphology (figure 7*b*). The 1 mGO (figure 7*e*) and 3 GO samples (figure 7*f*), with intermediate strain at break values, exhibited semi-fibrillar fracture morphology. Other samples, *viz*. 0.5 mGO (figure 7*c*), 1 GO (figure 7*d*) and 3 mGO (figure 7*g*), showed reduced ductility. The visible difference in the surface morphology of the fracture surfaces showed that the amount of GO loading and modification of GO influence the ductility as measured by strain at break values.

3.6. *In vitro* cytocompatibility

The cytocompatibility properties of the synthesized nanocomposites towards C2C12 murine myoblast cell viability, proliferation and attachment were analysed using WST-1 assay, fluorescence microscopy and SEM, respectively.

3.6.1. Cell proliferation and adhesion

Hoechst binds to the double-stranded deoxyribonucleic acid and gives an emission at blue wavelength, when excited at 340 nm [6]. The nuclei of cells stained with Hoechst on the control, HU, 1 GO and 1 mGO samples are shown in figure 8*a–d*, respectively. The total number of cells, counted over different nanocomposite substrates at the end of 3 days in culture observed using fluorescence imaging, were in the

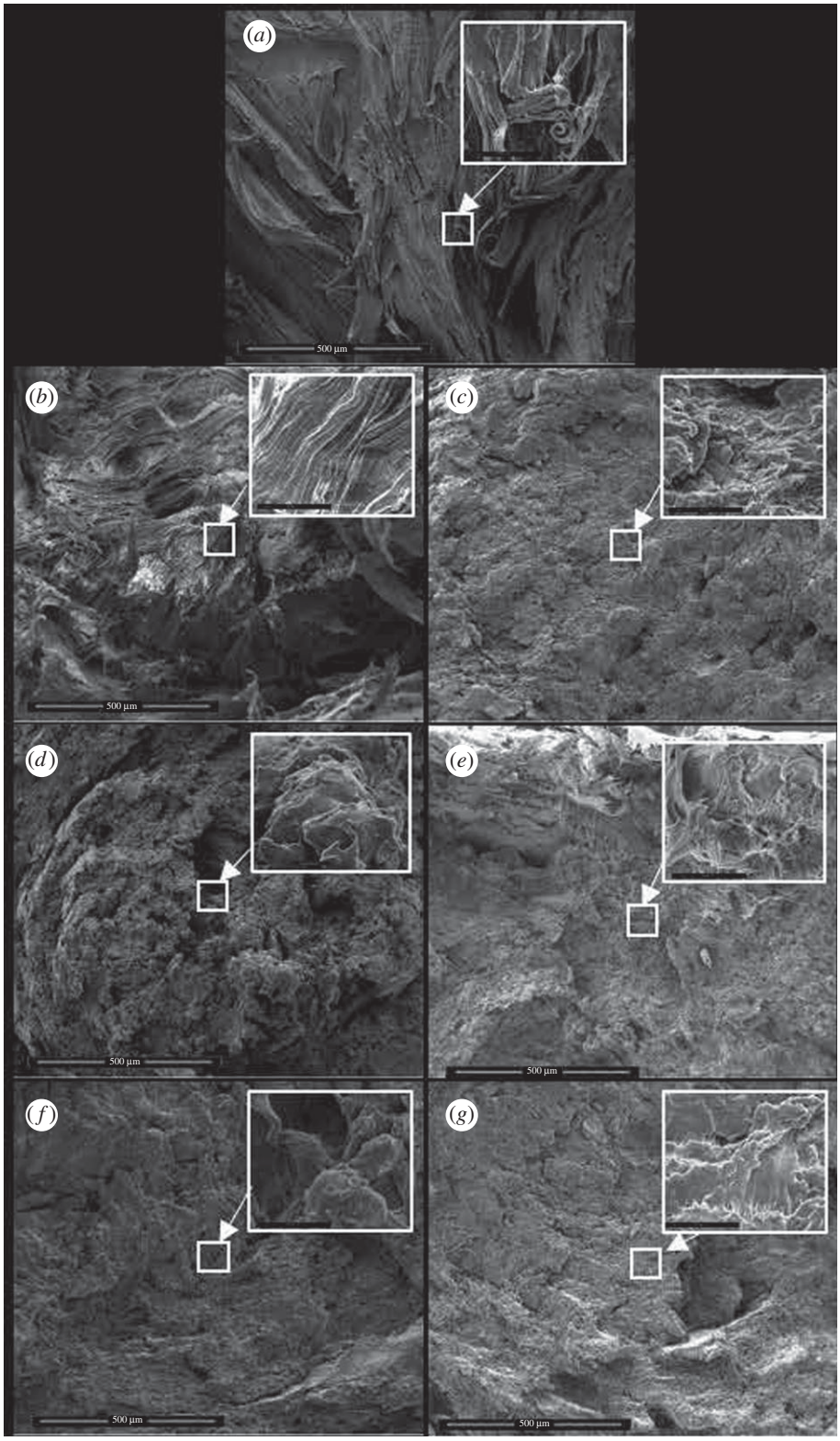

Figure 7. Fracture surface morphology of the GO/mGO-reinforced HU blend shows a change in its fracture behaviour. FESEM images of the tensile fractured surfaces of the nanocomposites: (*a*) HU; (*b*) 0.5 GO; (*c*) 0.5 mGO; (*d*) 1 GO; (*e*) 1 mGO; (*f*) 3 GO; (*g*) 3 mGO. For the material grade compositions mentioned in the figure, refer to table 1. (Scale bar: 500 µm, inset scale bar: 10 µm.)

range of 1.5–2 $\times$ 10^6 with no significant difference within the nanocomposites (figure 9*a*). We can thus say that nanocomposite substrates support the cell growth of the myoblast cells as good as the control sample.

The SEM micrographs of C2C12 myoblast cell adhesion on the control, HU, 1 GO and 1 mGO samples after 3 days of culture are shown in figure 8*e–h*. The adhesion of the cells was found to be normal on all the samples. The cultured cells appeared to have a strong attachment to the polymeric surface and also showed good cell to cell contact with the neighbouring cells.

3.6.2. Cell viability

In the WST-1 assay, the tetrazolium salt of WST-1 is converted to produce a coloured product by the mitochondrial dehydrogenase enzymes [6]. The change in OD is correlated with the number of viable cells [55]. The results of the

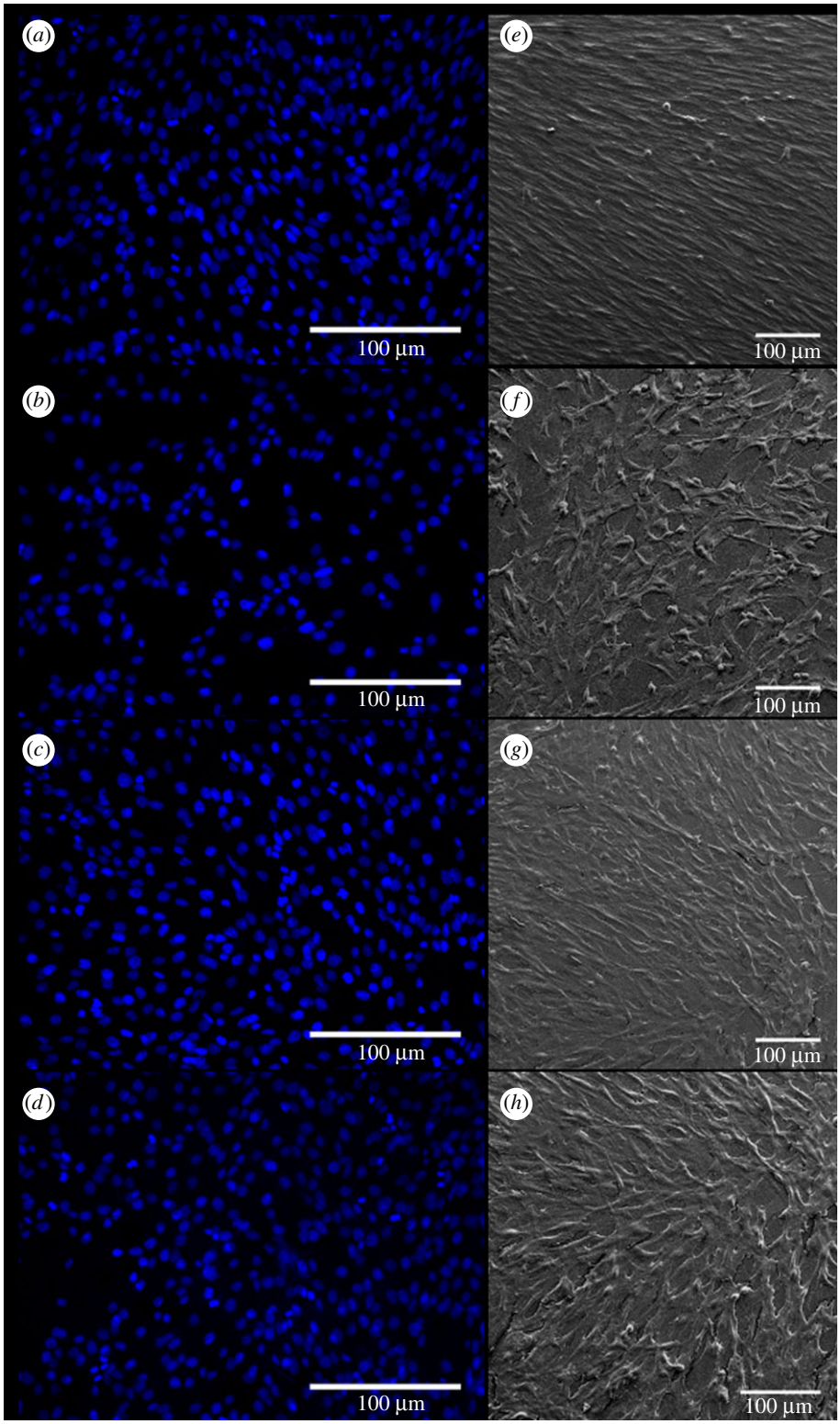

Figure 8. GO/mGO reinforcement does not compromise cell proliferation and adhesion of muscle cells on the polymeric substrates. Fluorescence microscopy images of C2C12 muscle cell nuclei after Hoechst staining at day 3 on (*a*) control, (*b*) HU, (*c*) 1 GO and (*d*) 1 mGO substrates; SEM micrographs showing C2C12 murine myoblast cell adhesion and cell-to-cell contact on (*e*) control, (*f*) HU, (*g*) 1 GO and (*h*) 1 mGO substrates. (Scale bar: 100 µm.) (Online version in colour.)

absorbance measurement of WST-1 assay are presented in figure 9*b*, which shows the proliferation of C2C12 murine myoblast cells on different nanocomposites at time points of 1 and 3 days in culture. The statistical test ANOVA confirmed the absence of any significant difference in the cell viability on the HU, 1 GO and 1 mGO samples, when compared with control at both the time intervals. The myoblast cell proliferation on the HU, 1 GO and 1 mGO samples was comparable to that on the control sample for the day 1 and day 3 readings. The addition of 1 wt% GO and mGO to the HU blend did not affect the growth of myoblast cells, when compared with the control substrate.

4. Discussion

The reinforcement of inorganic nanofillers (e.g. GO) in polymeric composites has been considered as an attractive strategy in the development of biomedical devices over the

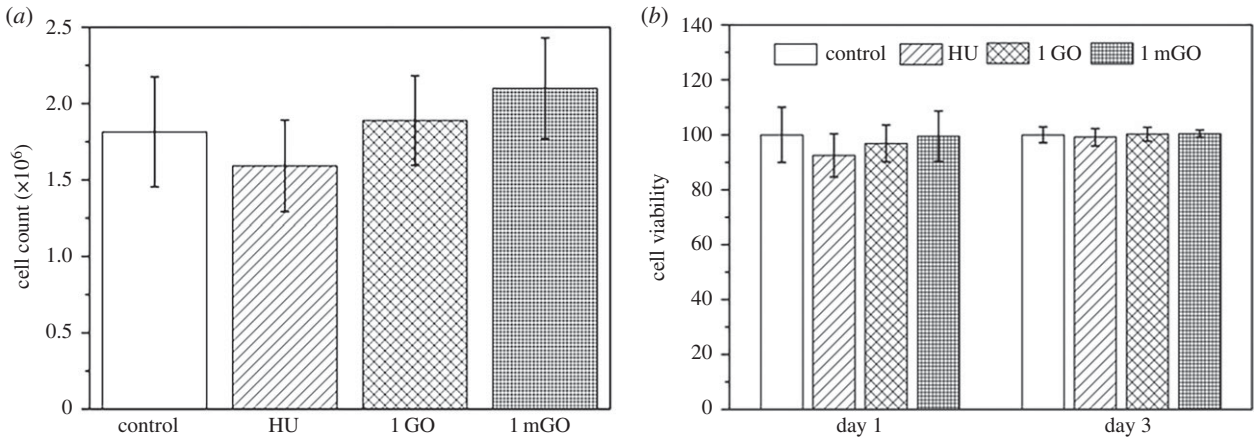

Figure 9. Quantitative analysis of cell viability provides complimentary evidence of cytocompatibility. (*a*) Cell count and (*b*) WST-1 assay plot showing cell viability of C2C12 murine myoblasts cells on various nanocomposites. One-way ANOVA was conducted for statistical analysis.

last decade [14]. In the present study, we establish that the 'dual' hybrid approach, involving surface modification of GO nanoparticles with mPE, efficiently disperses them in the HDPE/UHMWPE polymer blend. This allows one to obtain better mechanical properties and cytocompatibility of the nanocomposite. The surface modification was evaluated using techniques like FTIR, XRD and TGA while TEM and μ-CT images were used to check the dispersion of GO and mGO nanofillers in the polymer blend. Mechanical property enhancement was evaluated using uniaxial tension tests and compared to the Halpin–Tsai theoretical model. Further, C2C12 murine myoblast cells were used to assess their viability, proliferation and adhesion on the nanocomposites.

4.1. Surface modification of graphene oxide nanosheets

We adopted the chemical synthesis route of amine-functionalizing GO nanosheets by PEI, followed by mPE grafting. While the FTIR and Raman spectroscopy studies proved qualitatively the successful conjugation of the amine groups and the polyethylene grafting on the GO nanosheets. The shift in peaks observed in Raman spectroscopy and increase in the intensity ratio (I_D/I_G) w.r.t. neat GO corresponds to the increase in defect concentration which is due to introduction of functional groups onto GO sheets on modification with PEI and mPE [34]. However, the successful intercalation of PEI and maleated PE over GO can be quantified with the increasing *d*-spacing with the help of XRD. TGA results quantitatively showed the amount of polyethylene grafting on the GO nanosheets to be *ca* 63.8%. The surface wettability of the nanocomposite is also altered due to the surface modification of the GO nanosheets to mGO (discussed in the electronic supplementary material). It was observed that due to the presence of hydrophobic polyethylene wrapped over GO (mPE grafted over GO–PEI), the hydrophobicity of the mGO-reinforced nanocomposites increased. It is therefore quite likely that the hydrophilic groups (e.g. C–O, C=O, etc.) on GO are no more exposed due to PE grafting, resulting in an increase in hydrophobicity after reinforcement with mGO [56,57]. This increase in hydrophobicity was also confirmed by the TGA profile of mGO. Although the hydrophobicity of the mGO–HU surface increases relative to the GO–HU, the contact angle still remains in the range for hydrophilic surfaces (less than 90°) and thus supports the growth and proliferation of cells on the surface of the substrate.

4.2. Dispersion of graphene oxide/modified graphene oxide nanofillers and mechanical properties

For the design of devices such as hip acetabular implants, mechanical stability as well as optimal integration with the surrounding tissue region are of great significance [5]. Clinically used medical grade UHMWPE has been reported to have an ultimate tensile strength ranging from 42 to 44 MPa, whereas the elastic modulus varies from 1 to 1.39 GPa [58]. Thus, tensile properties of unmodified and modified graphene-reinforced HU blend were tested in an effort to match them to that of the natural bone and clinically used implant materials.

The rheological behaviour of GO–HU and mGO–HU nanocomposites, as observed from the complex frequency versus angular frequency graph, depicts that the viscosity decreased after surface modification of GO nanofillers. This manifested in a physical plasticizing effect caused by short molecular chains of mPE grafted over GO, as rheological properties are affected by molecular geometry and nature of the filler [59]. Thus, there is a reduction in viscosity of the nanocomposites reinforced with mGO, facilitating its better dispersion in the melt-mixed HU blend matrix [60].

The similarity in the observed mechanical properties of the 0.5 GO nanocomposite and the HU blend can be attributed to the agglomeration or restacking of unmodified GO nanoparticles within the HU polymer matrix caused due to hydrogen bonding or electrostatic interactions. The poor interaction of polar GO with the non-polar HU matrix leads to agglomeration and inferior dispersion of unmodified GO, which can be well inferred from the optical micrographs (electronic supplementary material, figure S3b), transmission electron micrographs (figure 4*a*) and volume rendered μ-CT imaging (figure 5*a*). Three-dimensional imaging from μ-CT revealed the volume distribution of nanoparticles in the polymer matrix. The nanoparticles and the polymer matrix are of different densities and different attenuation coefficients and therefore, the attenuation of X-rays is different for each component [61,62]. The grafting of maleated PE over GO modified with PEI facilitates the dispersion in the HU matrix along with lesser agglomeration, as can be clearly seen from the TEM images (figure 4*b*). The uniform dispersion of nanofiller in the matrix is an important aspect to effectively tune the property of the matrix. The sharp enhancement in the mechanical properties of the 1 mGO nanocomposite is due to the uniform dispersion of polyethylene-grafted mGO in the HU

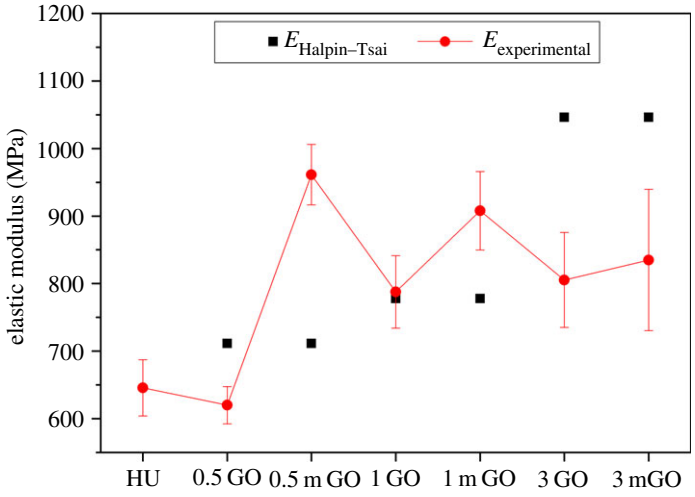

Figure 10. Theoretical elastic modulus values predicted by the Halpin–Tsai model compared to the experimentally calculated elastic modulus. (Online version in colour.)

blend polymer matrix, as seen in electronic supplementary material, figure S3*c*; figures 4*b* and 5*b* [63]. The uniform dispersion of nanoparticles in 1 mGO shows that the surface modification of GO with mPE leads to better dispersion, less agglomeration and better compatibilization in the matrix. All these attributes result in an enhancement of mechanical properties of the mGO–HU nanocomposites. This dispersion behaviour also led to the difference in the tensile fracture morphology of the nanocomposites. Better dispersion in the HU blend, as observed in the 1 mGO sample, showed a relatively fibrous morphology.

The uniform dispersion, leading to the improvement in the tensile properties, can be also attributed to the efficient mixing in the melt extruder, enabled by a recirculation channel, when compared with other techniques like solvent blending [40]. The other advantages of the melt-extrusion and injection moulding process included high shear rates for mGO dispersion, fabrication time within minutes and possibility of different shapes. The large shear forces present in the melt extruder allowed the dispersion of mGO particles without the need of surfactants. The polyethylene grafting on GO has resulted in an improved interfacial adhesion and thus improving the stress transfer from the matrix to the GO fillers, augmenting the mechanical properties. The mechanical properties also largely depend on the crystallinity of the polymer. Thus, a higher degree of crystallinity (*ca* 59%) of the 1 mGO sample corroborates the observed higher ultimate tensile strength and elastic modulus. This 'dual' hybrid modification to fabricate the 1 mGO nanocomposite led to a nearly 51% increase in the ultimate tensile strength as well as closely matched the elastic modulus when compared with the medical grade UHMWPE implants used clinically [58]. A further increase in the GO and mGO nanofiller loading to 3%, however, reduced ultimate tensile strength and elastic modulus, reflecting the reduced degree of crystallinity. This reduction in the mechanical performance can be attributed to the saturation of the HU blend matrix to efficiently disperse the GO and mGO fillers [64].

4.3. Correlation with theoretical prediction

The overall properties of the composite depend on both: the filler material and the matrix. Various theoretical models have been postulated to predict the individual contribution of the filler materials as well as that of the matrix. Composite properties like elastic modulus, filler aspect ratio, volume fraction, etc., contribute to the overall performance and those are considered in the theoretical models [65]. Such models include those given by Halpin and Tsai, Mori and Tanaka, Jager and Fratzl, etc. [66]. The Jager–Fratzl model predicts the elastic modulus of nacre-like biocomposites [66], whereas the Mori–Tanaka model involves solving a complex Eshelby tensor for a good estimate [65]. We used the Halpin–Tsai model for our study,

$$\mathrm{E}_{\text{Halpin–Tsai}} = \left(\frac{1 + \zeta\eta\varphi\mathrm{GO}}{1 - \eta\varphi\mathrm{GO}}\right) \times E_{\mathrm{HU}}$$

Here, $\mathrm{E}_{\text{Halpin–Tsai}}$ is the theoretical composite modulus, E_{HU} is the experimentally calculated elastic modulus of the HU matrix, ζ is the shape parameter dependent upon filler geometry, φ_{GO} is the volume fraction of the GO filler and η is given as follows:

$$\eta = \frac{(E_{\mathrm{GO}}/E_{\mathrm{HU}}) - 1}{(E_{\mathrm{GO}}/E_{\mathrm{HU}}) + \zeta}$$

where E_{GO}, elastic modulus of GO nanofillers, was taken to be 32 GPa [67]. It is safe to assume that the geometry of the GO nanofillers as rectangular sheets and the ζ was thus taken to be equal to w/t, where w is the width while t is the thickness of the nanosheets. φGO was calculated taking into account the density of the GO nanofillers (1.8881 g ml^{-1}) and the HU matrix (0.9288 g ml^{-1}) found using a helium gas pycnometer.

Figure 10 demonstrates the comparison between the theoretically predicted elastic modulus using the Halpin–Tsai model ($E_{\text{Halpin–Tsai}}$) and the experimental elastic modulus values ($E_{\text{experimental}}$) for respective composites. We see that the Halpin–Tsai model provided a good prediction for the elastic modulus of the 1 GO and 1 mGO nanocomposites, and it is useful in evaluating the mechanical properties coarsely. However, we also see that $E_{\text{experimental}}$ for the 3 GO and 3 mGO nanocomposites are significantly lower than the $E_{\text{Halpin–Tsai}}$ predicted. This is due to the fact that the Halpin–Tsai model overestimated the elastic modulus, while ignoring agglomeration and particle–particle interaction of GO nanofillers and interfaces in the nanocomposites [66]. Also, the model assumes an ideal non-slipping boundary condition, sharp interface between the filler and matrix, unidirectional filler orientation and isotropic matrix. The deviation from this

model assumption can explain the observed mismatch between the experimental values and model predictions [65,66]. It is also important to note that the shape parameter ζ, calculated using the AFM imaging data of the pristine GO nanosheets, was assumed to be constant for all the loading percentages. This may not be the case practically, thus leading to the difference.

4.4. Influence of graphene oxide/modified graphene oxide reinforcement on cellular behaviour

Graphene-based materials have been shown to be cytocompatible with skeletal muscle cells [68]. The samples were checked for their *in vitro* cytocompatibility using WST-1 assay, fluorescence imaging and SEM analysis. The results (figures 8 and 9) reflect the signature of promising response from the C2C12 murine myoblast cells on the polymeric substrates. The interaction between the cells and nanofiller-reinforced polymer substrates depends on various factors like fabrication processes, dispersion of the nanofillers in the polymer matrix, functional groups on the nanofillers, surface wettability, etc. [14]. The WST-1 assay as well as the cell count calculated using fluorescence imaging suggests that the cells proliferate as good on the modified polymeric substrates as on the control. Also, the cell adhesion on the substrates together with good cell-to-cell interaction after 3 days in culture, observed using SEM micrographs, further proves that the cytocompatibility is not compromised with the addition of mGO. The cellular viability results also rule out the possibility of the potential release of PEI into the culture medium leading to toxicity. The cellular response by co-culture studies is also a critical strategy which allows the development of a model that can be evaluated at a physiologically relevant level [69]. In our previous study, we investigated the cellular response of hMSCs on HDPE-mGO composites [4]. Co-culture studies, especially with the currently used myoblast cells along with osteoblast cells or human mesenchymal stem cells, may provide interesting results and can be further explored in near future.

5. Conclusion

We report here a new processing strategy to covalently graft polyethylene chains onto GO nanosheets with a high grafting efficiency. The optimal loading of modified GO led to a better dispersion of the GO nanosheets and improved the processability, as assessed using melt-extrusion and injection moulding route. The 'dual' hybrid approach to prepare an HDPE/UHMWPE blend with a low weight percentage addition of surface-modified GO, resulted in superior mechanical properties compared to the clinically used UHMWPE. An optimized blend of 60 wt% HDPE/40 wt% UHMWPE, reinforced with 1 wt% mGO, Exhibited an increase in the ultimate tensile strength by 120% (*ca* 65 MPa) and elastic modulus by 40% (*ca* 908 MPa) compared to the neat blend. Moreover, the nanocomposites supported good skeletal muscle cell attachment and proliferation, *in vitro*. Thus, HDPE/UHMWPE/mGO hybrid nanocomposite could be a promising biomaterial for bone tissue engineering applications.

Data accessibility. No empirical data were used in this study and all simulated data and related scripts are provided as electronic supplementary material available for this publication.

Authors' contributions. S.A.B. has fabricated the blend as well as the nanocomposites through melt mixing and has carried out experiments including mechanical testing and cell viability assays. He has also participated in the design of the study and drafting of the manuscript. V.S. has undertaken characterization to qualitatively analyse the dispersion of nanofillers in the matrix with advanced techniques like TEM, μ-CT and rheometry. She has also participated in the design of the study and manuscript drafting. She has also undertaken experiments significant for further clarification during the revision of the manuscript and also incorporated those in the main document. S.B. being the polymer processing expert provided guidance throughout material selection, processing (including variation of parameters like pressure, temperature, torque, etc.), characterization and the result analyses. B.B. is the biomaterial scientist, and scientifically supervised the *in vitro* experiments, especially in understanding the cell material interactions. His suggestions were also very productive in establishing the mechanical model for the fabricated nanocomposites.

Competing interests. We declare we have no competing interests.

Funding. The present study is funded by Department of Biotechnology (grant no. BT/PR13466/COE/34/26/2015), Government of India, and 'Centres of Excellence and Innovation in Biotechnology' scheme through the Centre of Excellence Project, Translational Centre on Biomaterials for Orthopaedic and Dental Applications.

Acknowledgements. The authors are grateful to Department of Biotechnology Government of India, and 'Centres of Excellence and Innovation in Biotechnology' scheme through the Centre of Excellence Project, Translational Centre on Biomaterials for Orthopaedic and Dental Applications. The authors gratefully acknowledge support from Dr Nagendra Singh for TEM imaging at NCBS, Mr Sourav Mandal for SEM and μ-CT images and Mr Amannuel Gebrekrstos for rheology experiments.

References

1. Bosco R, Van Den Beucken J, Leeuwenburgh S, Jansen J. 2012 Surface engineering for bone implants: a trend from passive to active surfaces. *Coatings* **2**, 95–119. (doi:10.3390/coatings2030095)
2. Goodman SB, Yao Z, Keeney M, Yang F. 2013 The future of biologic coatings for orthopaedic implants. *Biomaterials* **34**, 3174–3183. (doi:10.1016/j.biomaterials.2013.01.074)
3. Basu B. 2017 *Biomaterials science and tissue engineering: principles and methods*. Cambridge, UK: Cambridge University Press.
4. Basu B, Ghosh S. 2017 *Biomaterials for musculoskeletal regeneration*. Berlin, Germany: Springer.
5. Bauer S, Schmuki P, von der Mark K, Park J. 2013 Engineering biocompatible implant surfaces. *Prog. Mater Sci.* **58**, 261–326. (doi:10.1016/j.pmatsci.2012.09.001)
6. Upadhyay R, Naskar S, Bhaskar N, Bose S, Basu B. 2016 Modulation of protein adsorption and cell proliferation on polyethylene immobilized graphene oxide reinforced HDPE bionanocomposites. *ACS Appl. Mater. Interfaces* **8**, 11 954–11 968. (doi:10.1021/acsami.6b00946)
7. Bougherara H, Bureau MN, Yahia LH. 2009 Bone remodeling in a new biomimetic polymer-composite hip stem. *J. Biomed. Mater. Res. A* **92**, 164–174. (doi:10.1002/jbm.a.32346)
8. Chen Y, Qi Y, Tai Z, Yan X, Zhu F, Xue Q. 2012 Preparation, mechanical properties and biocompatibility of graphene oxide/ultrahigh molecular weight polyethylene composites. *Eur. Polym. J.* **48**, 1026–1033. (doi:10.1016/j.eurpolymj.2012.03.011)
9. Deng M, Latour RA, Ogale AA, Shalaby SW. 1997 Study of creep behavior of ultra-high-molecular-weight polyethylene systems. *J. Biomed. Mater. Res. A* **40**, 214–223. (doi:10.1002/(SICI)1097-4636(199805)40:2<214::AID-JBM6>3.0.CO;2-0)
10. Maksimkin AV, Kharitonov AP, Mostovaya KS, Kaloshkin SD. 2016 Bulk oriented nanocomposites of ultrahigh molecular weight polyethylene

reinforced with fluorinated multiwalled carbon nanotubes with nanofibrillar structure. *Composites Part B* **94**, 292–298. (doi:10.1016/j.compositesb.2016.03.061)

11. Lin Y, Jin J, Song M. 2011 Preparation and characterisation of covalent polymer functionalized graphene oxide. *J. Mater. Chem.* **21**, 3455–3461. (doi:10.1039/c0jm01859g)
12. Xue Y, Wu W, Jacobs O, Schädel B. 2006 Tribological behaviour of UHMWPE/HDPE blends reinforced with multi-wall carbon nanotubes. *Polym. Test.* **25**, 221–229. (doi:10.1016/j.polymertesting.2005.10.005)
13. Ge S, Wang S, Huang X. 2009 Increasing the wear resistance of UHMWPE acetabular cups by adding natural biocompatible particles. *Wear* **267**, 770–776. (doi:10.1016/j.wear.2009.01.057)
14. Puértolas JA, Kurtz SM. 2014 Evaluation of carbon nanotubes and graphene as reinforcements for UHMWPE-based composites in arthroplastic applications: a review. *J. Mech. Behav. Biomed. Mater.* **39**, 129–145. (doi:10.1016/j.jmbbm.2014.06.013)
15. Lim KLK, Mohd Ishak ZA, Ishiaku US, Fuad AMY, Yusof AH, Czigany T, Pukanszky B, Ogunniyi DS. 2005 High-density polyethylene/ultrahigh-molecular-weight polyethylene blend. I. The processing, thermal, and mechanical properties. *J. Appl. Polym. Sci.* **97**, 413–425. (doi:10.1002/app.21298)
16. Sui G, Zhong WH, Ren X, Wang XQ, Yang XP. 2009 Structure, mechanical properties and friction behavior of UHMWPE/HDPE/carbon nanofibers. *Mater. Chem. Phys.* **115**, 404–412. (doi:10.1016/j.matchemphys.2008.12.016)
17. Wang Q, Liu J, Ge S. 2009 Study on biotribological behavior of the combined joint of CoCrMo and UHMWPE/BHA composite in a hip joint simulator. *J. Bionic Eng.* **6**, 378–386. (doi:10.1016/s1672-6529(08)60139-0)
18. Plumlee K, Schwartz CJ. 2009 Improved wear resistance of orthopaedic UHMWPE by reinforcement with zirconium particles. *Wear* **267**, 710–717. (doi:10.1016/j.wear.2008.11.028)
19. Bigsby RJA, Auger DD, Jin ZM, Dowson D, Hardaker CS, Fisher J. 1998 A comparative tribological study of the wear of composite cushion cups in a physiological hip joint simulator. *J. Biomech.* **31**, 363–369. (doi:10.1016/S0021-9290(98)00034-7)
20. Zhang BGX, Myers DE, Wallace GG, Brandt M, Choong PFM. 2014 Bioactive coatings for orthopaedic implants—recent trends in development of implant coatings. *Int. J. Mol. Sci.* **15**, 11 878–11 921. (doi:10.3390/ijms150711878)
21. Goodman SB *et al.* 2014 Novel biological strategies for treatment of wear particle-induced periprosthetic osteolysis of orthopaedic implants for joint replacement. *J. R. Soc. Interface* **11**, 20130962. (doi:10.1098/rsif.2013.0962)
22. Pang H, Piao YY, Cui CH, Bao Y, Lei J, Yuan GP, Zhang CL. 2013 Preparation and performance of segregated polymer composites with hybrid fillers of octadecylamine functionalized graphene and carbon nanotubes. *J. Polym. Res.* **20**, 304. (doi:10.1007/s10965-013-0304-4)
23. Yang BX, Pramoda KP, Xu GQ, Goh SH. 2007 Mechanical reinforcement of polyethylene using polyethylene-grafted multiwalled carbon nanotubes. *Adv. Funct. Mater.* **17**, 2062–2069. (doi:10.1002/adfm.200600599)
24. Kumar S, Raj S, Kolanthai E, Sood AK, Sampath S, Chatterjee K. 2015 Chemical functionalization of graphene to augment stem cell osteogenesis and inhibit biofilm formation on polymer composites for orthopedic applications. *ACS Appl. Mater. Interfaces* **7**, 3237–3252. (doi:10.1021/am5079732)
25. Fang L, Leng Y, Gao P. 2006 Processing and mechanical properties of HA/UHMWPE nanocomposites. *Biomaterials* **27**, 3701–3707. (doi:10.1016/j.biomaterials.2006.02.023)
26. Liu J, Cui L, Losic D. 2013 Graphene and graphene oxide as new nanocarriers for drug delivery applications. *Acta Biomater.* **9**, 9243–9257. (doi:10.1016/j.actbio.2013.08.016)
27. Yang Y, Asiri AM, Tang Z, Du D, Lin Y. 2013 Graphene based materials for biomedical applications. *Mater. Today* **16**, 365–373. (doi:10.1016/j.mattod.2013.09.004)
28. Puvirajesinghe TM, Zhi ZL, Craster RV, Guenneau S. 2018 Tailoring drug release rates in hydrogel-based therapeutic delivery applications using graphene oxide. *J. R. Soc. Interface* **15**, 20170949. (doi:10.1098/rsif.2017.0949)
29. Kim H, Namgung R, Singha K, Oh IK, Kim WJ. 2011 Graphene oxide–polyethylenimine nanoconstruct as a gene delivery vector and bioimaging tool. *Bioconjug. Chem.* **22**, 2558–2567. (doi:10.1021/bc200397j)
30. Matharu RK, Porwal H, Ciric L, Edirisinghe M. 2018 The effect of graphene–poly(methyl methacrylate) fibres on microbial growth. *Interface Focus* **8**, 20170058. (doi:10.1098/rsfs.2017.0058)
31. Banerjee AN. 2018 Graphene and its derivatives as biomedical materials: future prospects and challenges. *Interface Focus* **8**, 20170056. (doi:10.1098/rsfs.2017.0056)
32. Yao G, Duan T, An M, Xu H, Tian F, Wang Z. 2017 The influence of epitaxial crystallization on the mechanical properties of a high density polyethylene/reduced graphene oxide nanocomposite injection bar. *RSC Adv.* **7**, 21 918–21 925. (doi:10.1039/c7ra02742g)
33. Dreyer DR, Park S, Bielawski W, Ruoff RS. 2010 The chemistry of graphene oxide. *Chem. Soc. Rev.* **39**, 228–240. (doi:10.1039/b917103g)
34. Wan YJ, Tang LC, Gong LX, Yan D, Li YB, Wu LB, Jiang JX, Lai GQ. 2014 Grafting of epoxy chains onto graphene oxide for epoxy composites with improved mechanical and thermal properties. *Carbon* **69**, 467–480. (doi:10.1016/j.carbon.2013.12.050)
35. Shen B, Zhai W, Tao M, Lu D, Zheng W. 2013 Chemical functionalization of graphene oxide toward the tailoring of the interface in polymer composites. *Compos. Sci. Technol.* **77**, 87–94. (doi:10.1016/j.compscitech.2013.01.014)
36. Fang M, Wang K, Lu H, Nutt S. 2009 Covalent polymer functionalization of graphene nanosheets and mechanical properties of composites. *J. Mater. Chem.* **19**, 7098–7105. (doi:10.1039/b908220d)
37. Heseltine PL, Ahmed J, Edirisinghe M. 2018 Developments in pressurized gyration for the mass production of polymeric fibers. *Macromol. Mater. Eng.* **303**, 1800218. (doi:10.1002/mame.201800218)
38. Medina C, Daurio D, Nagapudi K, Alvarez-nunez F. 2010 Manufacture of pharmaceutical co-crystals using twin screw extrusion: a solvent-less and scalable process. *J. Pharm. Sci.* **99**, 1693–1696. (doi:10.1002/jps)
39. Breitenbach J. 2002 Melt extrusion: from process to drug delivery technology. *Eur. J. Pharm. Biopharm.* **54**, 107–117. (doi:10.1016/S0939-6411(02)00061-9)
40. Maniruzzaman M, Boateng JS, Snowden MJ, Douroumis D. 2012 A review of hot-melt extrusion: process technology to pharmaceutical products. *ISRN Pharm.* **2012**, 436763. (doi:10.5402/2012/436763)
41. Tzoganakis C. 1989 Reactive extrusion of polymers: a review. *Adv. Polym. Technol.* **9**, 321–330.
42. Wang F, Liu L, Xue P, Jia M. 2017 Crystal structure evolution of UHMWPE/HDPE blend fibers prepared by melt spinning. *Polymers* **9**, 96. (doi:10.3390/polym9030096)
43. Cimmino S, Di Pace E, Martuscelli E, Silvestre C, Mendes LC, Bonfanti G. 1995 High density polyethylene/hydrogenated oligo (cyclopentadiene) blends: tensile stress–strain behavior. *J. Polym. Sci. Part B Polym. Phys.* **33**, 1723–1730.
44. Patel AK, Trivedi P, Balani K. 2014 Processing and mechanical characterization of compression-molded ultrahigh molecular weight polyethylene biocomposite reinforced with aluminum oxide. *J. NanoSci., Nanoeng. Appl.* **4**, 1–11.
45. Katti P, Kundan KV, Kumar S, Bose S. 2017 Improved mechanical properties through engineering the interface by poly (ether ether ketone) grafted graphene oxide in epoxy based nanocomposites. *Polymer (UK)* **122**, 184–193. (doi:10.1016/j.polymer.2017.06.059).
46. She X, Liu T, Wu N, Xu X, Li J, Yang D, Frost R. 2013 Spectrum analysis of the reduction degree of two-step reduced graphene oxide (GO) and the polymer/r-GO composites. *Mater. Chem. Phys.* **143**, 240–246. (doi:10.1016/j.matchemphys.2013.08.059)
47. Navaee A, Salimi A. 2015 Efficient amine functionalization of graphene oxide through the Bucherer reaction: an extraordinary metal-free electrocatalyst for the oxygen reduction reaction. *RSC Adv.* **5**, 59 874–59 880. (doi:10.1039/c5ra07892j)
48. Sharma M, Madras G, Bose S. 2015 Contrasting effects of graphene oxide and poly(ethylenimine) on the polymorphism in poly(vinylidene fluoride). *Cryst. Growth Des.* **15**, 3345–3355. (doi:10.1021/acs.cgd.5b00445)
49. Liu J, Ma D, Li Z. 2002 FTIR studies on the compatibility of hard-soft segments for polyurethane–imide copolymers with different soft segments. *Eur. Polym. J.* **38**, 661–665. (doi:10.1016/s0014-3057(01)00247-6)

50. Yeganeh H, Shamekhi MA. 2004 Poly(urethane-imide-imide), a new generation of thermoplastic polyurethane elastomers with enhanced thermal stability. *Polymer* **45**, 359–365. (doi:10.1016/j.polymer.2003.11.006)
51. Huang H-D, Zhou S-Y, Ren PG. 2015 Improved mechanical and barrier properties of low-density polyethylene nanocomposite films by incorporating hydrophobic graphene oxide nanosheets. *RSC Adv.* **5**, 80 739–80 748. (doi:10.1039/c5ra12694k)
52. Li Y, Li X. 2010 A graphene oxide-based molecularly imprinted polymer platform for detecting endocrine disrupting chemicals. *Carbon* **48**, 3427–3433. (doi:10.1016/j.carbon.2010.05.038)
53. Lou X, Detrembleur C, Sciannamea V, Pagnoulle C, Jérôme R. 2004 Grafting of alkoxyamine end-capped (co) polymers onto multi-walled carbon nanotubes. *Polymer* **45**, 6097–6102. (doi:10.1016/j.polymer.2004.06.050)
54. Jaggi HS, Satapathy BK, Ray AR. 2014 Viscoelastic properties correlations to morphological and mechanical response of HDPE/UHMWPE blends. *J. Polym. Res.* **21**, 482. (doi:10.1007/s10965-014-0482-8)
55. Bhaskar N, Padmavathy N, Jain S, Bose S, Basu B. 2016 Modulated *in vitro* biocompatibility of a unique cross-linked salicylic acid-poly(ε-caprolactone)-based biodegradable polymer. *ACS Appl. Mater. Interfaces* **8**, 29 721–29 733. (doi:10.1021/acsami.6b10711)
56. Wu S, Ran Q, Liu Z. 2007 Studies on structure and properties of HDPE functionalized through ultraviolet irradiation and its blends with $CaCO_3$. *Polymer-Plast. Technol. Eng.* **44**, 1467–1474. (doi:10.1081/200048521)
57. Maria D, Airinei A, Homocianu M, Fifere N, Timpu D, Magdalena A. 2013 Structural characteristics of some high density polyethylene/EPDM blends. *Polym. Test.* **32**, 187–196. (doi:10.1016/j.polymertesting.2012.10.010)
58. Pruitt LA. 2005 Deformation, yielding, fracture and fatigue behavior of conventional and highly cross-linked ultra high molecular weight polyethylene. *Biomaterials* **26**, 905–915. (doi:10.1016/j.biomaterials.2004.03.022)
59. Bose S, Bhattacharyya AR, Kulkarni AR, Pötschke P. 2009 Electrical, rheological and morphological studies in co-continuous blends of polyamide 6 and acrylonitrile–butadiene–styrene with multiwall carbon nanotubes prepared by melt blending. *Compos. Sci. Technol.* **69**, 365–372. (doi:10.1016/j.compscitech.2008.10.024)
60. Nandi S, Bose S, Mitra S, Ghosh AK. 2012 Dynamic rheology and morphology of HDPE-fumed silica composites: effect of interface modification. *Polym. Eng. Sci.* **53**, 644–650. (doi:10.1002/pen.23299)
61. Kumar S, Raj S, Jain S, Chatterjee K. 2016 Multifunctional biodegradable polymer nanocomposite incorporating graphene–silver hybrid for biomedical applications. *Mater. Des.* **108**, 319–332. (doi:10.1016/j.matdes.2016.06.107)
62. Busignies V, Leclerc B, Porion P, Evesque P, Couarraze G, Tchoreloff P. 2006 Quantitative measurements of localized density variations in cylindrical tablets using X-ray microtomography. *Eur. J. Pharm. Biopharm.* **64**, 38–50. (doi:10.1016/j.ejpb.2006.02.007)
63. Cai Z, Meng X, Han Y, Ye H, Cui L, Zhou Q. 2015 Reinforcing polyamide 1212 with graphene oxide via a two-step melt compounding process. *Compos. Part A* **69**, 115–123. (doi:10.1016/j.compositesa.2014.11.011)
64. Suñer S, Joffe R, Tipper JL, Emami N. 2015 Ultra high molecular weight polyethylene/graphene oxide nanocomposites: thermal, mechanical and wettability characterisation. *Compos. Part B: Eng.* **78**, 185–191. (doi:10.1016/j.compositesb.2015.03.075)
65. Fornes TD, Paul DR. 2003 Modeling properties of nylon 6/clay nanocomposites using composite theories. *Polymer* **44**, 4993–5013. (doi:10.1016/s0032-3861(03)00471-3)
66. Hu K, Kulkarni DD, Choi I, Tsukruk VV. 2014 Graphene-polymer nanocomposites for structural and functional applications. *Prog. Polym. Sci.* **39**, 1934–1972. (doi:10.1016/j.progpolymsci.2014.03.001)
67. Compton OC, Nguyen ST. 2010 Graphene oxide, highly reduced graphene oxide, and graphene: versatile building blocks for carbon-based materials. *Small* **6**, 711–723. (doi:10.1002/smll.200901934)
68. Ryon S *et al.* 2016 Graphene-based materials for tissue engineering. *Adv. Drug Deliv. Rev.* **105**, 255–274. (doi:10.1016/j.addr.2016.03.007).
69. Lu HH, Subramony SD, Boushell MK, Zhang X. 2010 Tissue engineering strategies for the regeneration of orthopedic interfaces. *Ann. Biomed. Eng.* **38**, 2142–2154. (doi:10.1007/s10439-010-0046-y)